

Crop classification using object-oriented method and Google Earth Engine

Geeta T. Desai¹, Abhay N. Gaikwad²

¹Department of Electronics and Computer Science, Anjuman-I-Islam's Kalsekar Technical Campus, Mumbai University, Panvel, India

²Department of Electronics, Babasaheb Naik College of Engineering, Pusad, India

Article Info

Article history:

Received May 8, 2024

Revised Oct 25, 2024

Accepted Nov 14, 2024

Keywords:

Crop classification
Google Earth Engine
Machine learning
Sentinel-1
Sentinel-2

ABSTRACT

Agriculture crop monitoring in real-time is crucial in formulating effective agricultural practices and management policies. The primary goal of the investigation is to explore how the utilization of Sentinel-1 data and its fusion with Sentinel-2 impact crop classification accuracy in a fragmented agricultural landscape in the Yavatmal District of Maharashtra, India. Pixel based classification and object-oriented classification approaches were implemented on Google Earth Engine (GEE), and obtained results were compared for different combinations of optical and microwave features. The research revealed that the object-based technique performed better than the pixel-based approach, with a 3.5% increase in overall accuracy. For 2022, crop-type mapping was generated with overall accuracies varying from 85.5% to 61% and a kappa coefficient between 0.77 and 0.37. These overall accuracies imply that joint use of optical and radar data has given a 24% improvement in overall accuracy compared to use of only optical data. In addition, the temporal change in the backscatter coefficients and different vegetation indices for different crops were examined over crop growth cycle. This work demonstrates the fusion of Sentinel-1 and Sentinel-2 data to classify wheat, chickpea, other crops, water and urban areas.

This is an open access article under the [CC BY-SA](#) license.



Corresponding Author:

Geeta T. Desai

Department of Electronics and Computer Science

Anjuman-I-Islam's Kalsekar Technical Campus, Mumbai University

New Panvel, Navi Mumbai, Maharashtra, India 410206

Email: tgeetadesai@gmail.com

1. INTRODUCTION

Eradicating hunger and ensuring food security are top priorities for humanity. Crop classification (CC) maps are vital for designing and implementing agricultural monitoring practices that ensure food security and deal with environmental challenges caused by global warming [1], [2]. While extensive farming is a global trend, smallholder farming is widespread in India, as a result, the performance of small and marginal farmers will determine the future of sustainable agricultural growth and food security in India [3]. In India, cropping patterns are highly diverse concerning the types of crops and their number per year, making classification a challenging task. The traditional method of sample surveys used to determine crop distribution is labor-intensive and requires substantial resources, and its quality and timeliness cannot always be guaranteed [4]. However, satellite remote sensing has shown a higher potential for creating accurate crop maps. With the introduction of the Copernicus program, which offers frequent and cost-effective observations in optical Sentinel-2 and microwave Sentinel-1 domains, satellite remote sensing has become an attractive alternative for determining accurate crop maps [5]. Dealing with the processing of massive volume of remote sensing data for large areas poses several challenges, including time-consuming tasks, high data

bandwidth requirements for downloading, and the need for fast computing and enormous storage capacity. Google Earth Engine (GEE) is a cloud-based platform that permits users to download and process remote sensing imagery quickly. GEE has become increasingly popular among researchers due to its availability of different machine learning algorithms and quick processing times [6], [7]. Previous studies have demonstrated significant progress in building machine learning-based CC algorithms utilizing remote sensing imagery [8], [9]. The random forest (RF) classifier is particularly popular among researchers due to its outstanding classification accuracy and high processing speed in remote sensing applications [10].

Cloud cover poses significant challenges when it comes to using optical remote sensing, but synthetic aperture radar (SAR) images with cloud penetration capabilities can overcome this issue. Optical data is an excellent choice for creating crop maps since it allows the calculation of vegetation indices and provides valuable information about the biophysical processes of vegetation. On the other hand, SAR backscattering echo can reflect structural information about the target, based on the frequency and polarization [11]. The combination of optical and microwave imagery can be deployed to get accurate crop mapping through fusion techniques. Many researchers have proposed the amalgamation of optical and microwave information for CC [12]–[16], but only a few have focused on small farmlands. While researchers have used object-oriented (OO) techniques to enhance CC accuracy [17]–[19], most of the work focuses on a single type of microwave or optical remote sensing images. Moreover, to the best of our knowledge, no research has yet explored the utilization of OO approach combined with the amalgamation of Sentinel-1 and Sentinel-2 imagery for small farmlands. The major objectives of research are:

- Evaluate mapping of crops with Sentinel-1 and Sentinel-2 data in regions having small-size farms using OO CC.
- Investigate the performance of OO and pixel-based (PB) technique for CC.
- Study normalized difference vegetation index (NDVI), green normalized difference vegetation index (GNDVI), normalized difference yellow index (NDYI), modified normalized difference water index (MNDWI), and backscatter temporal profiles of various crops.

The remaining paper is organized as follows: in section 2, we review the works related to CC, while section 3 provides information on data acquisition and the proposed methodology of the CC algorithm. In section 4, we present the obtained results for CC using different combinations of Sentinel-1 and Sentinel-2 data. Finally, in section 5, we summarize the future scope of the proposed research and our conclusions.

2. LITERATURE REVIEW

This section covers previous studies done by researchers for CC. Previous studies demonstrate the fusion and single sensor methods based on either optical or SAR data for crop mapping. Son *et al.* [20] demonstrated the application of a smooth backscattering profile for rice crop mapping using Sentinel-1A data. Nihar *et al.* [21] investigated the capacity of Sentinel-1 data for maize and corn crop area mapping using vertical-horizontal (VH) and vertical-vertical (VV) backscattering decision tree classifier recorded the accuracy of 75.0% for VH. In [22]–[24], deep learning methods were evaluated for CC using SAR data. Research by Kobayashi *et al.* [25], using the Sentinel-2 data authors, computed and evaluated 91 published spectral indices for CC and concluded that CC based on spectral indices gave good results. Saini and Ghosh [26] concluded that the NIR band in Sentinel-2 data played the most prominent role in CC results concluding that overall CC accuracy of Sentinel-2 imagery obtained by RF and support vector machine is 84.22% and 81.85%, respectively.

Sonobe *et al.* [27] concluded that for detailed crop mapping, vegetation indices calculated from the original reflectance of Sentinel-2 contributed significantly. Mazzia *et al.* [28] proposed the application of recurrent and convolution neural networks for land cover and CC using Sentinel-2 data. Sentinel-2 red edge band1 and shortwave infrared band1 had shown greater accuracy in crop mapping. The amalgamation of optical and SAR data offers a comprehensive representation of structural and biophysical information about objects, improving CC accuracy. Many researchers have used optical and SAR data integration for CC [12]–[16]. The above-mentioned CC methods are PB and perform CC by deriving the temporal optical or microwave features of image elements. PB CC techniques neglect the spatial correlation among adjacent pixel elements [29], due to which these techniques are sensitive to salt-and-pepper noise and have higher requirements for computing power [30]. The OO CC techniques based on remote sensing images can lower the salt-and-pepper noise [17], [18]. Yang *et al.* [19] demonstrate the potential of simple non-iterative clustering (SNIC) superpixel segmentation technique for high-resolution crop mapping based on Sentinel-1 data. A 10% increase in accuracy was obtained in [31] utilizing composite Sentinel-1 images and the OO categorization technique.

In conclusion, research combining optical and SAR characteristics of crop type mapping has received much attention. The following possible set of concerns has been found in previous research work:

- Many researchers have proposed the amalgamation of optical and microwave information for CC, but only a few have focused on small farmlands.
- Most current studies on heterogeneous farmlands are based on PB CC method which suffer from salt and pepper noise.
- Most of the work focuses on a single type of microwave or optical remote sensing images. There has been less attention given to the advantages that can be obtained by fusing different types of images.

The proposed work exploits OO approach fusion of SAR and optical data for CC. The experiment is focused on smallholder agricultural landscapes in rural Maharashtra.

3. METHOD

The Figure 1 illustrates the adapted methodological approach for CC in the investigation area, which involves using various features extracted from Sentinel-1 and Sentinel-2 data. The approach comprises four main steps: i) acquisition and preprocessing of Sentinel-1 and Sentinel-2 data, ii) data preparation, where vegetation indices are calculated from time series optical and SAR images, iii) CC, where extracted optical and SAR features are merged, and CC is performed using OO and PB approach in different scenarios on GEE platform using RF classifier, and iv) accuracy assessment of the resulting classified maps.

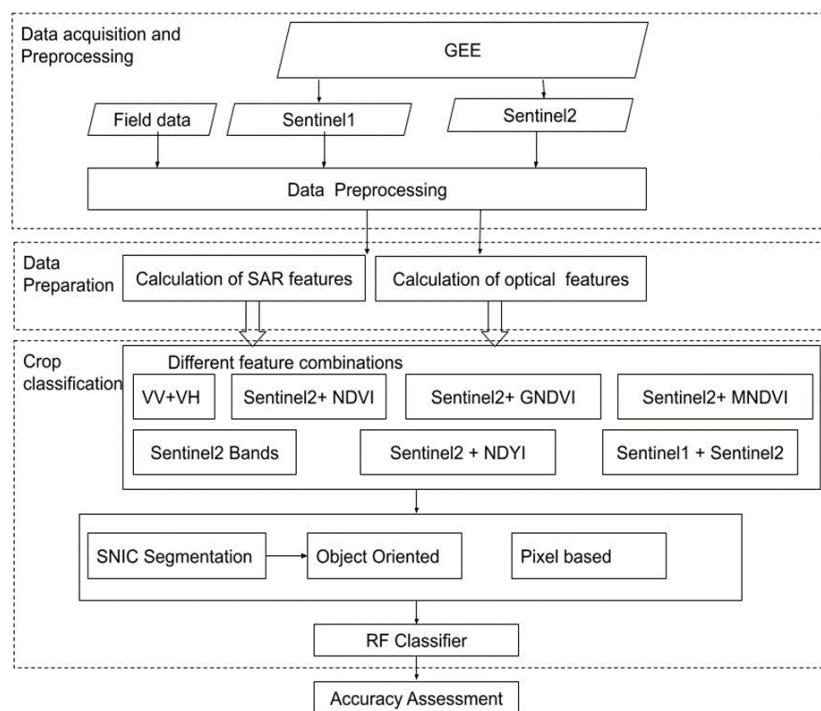


Figure 1. Flowchart of methodology

3.1. Sentinel-1 and Sentinel-2 data acquisition and preprocessing

The study encompasses an area of around 743 km² with 70% of the land dedicated to agriculture. The landscape is heterogeneous and complex, with chickpeas and wheat being the dominant crops grown. The agricultural area is mostly composed of small farms that are less than a hectare in size. The study area is situated at latitude 19.912676 and longitude 77.566910. The soil in the area has a clayey loamy texture and is somewhat alkaline, containing calcium carbonate. The climate in the area is hot and dry during the summer, with a mean maximum temperature of 41 °C in May and a temperature range of 12-22 °C in winter. The annual rainfall in the region is typically between 850 and 1,150 mm. The study area includes the villages of Warud and Bhujla in Pusad, where agriculture is a primary source of income.

3.1.1. Sentinel-1 data acquisition and preprocessing

The study utilized a combination of optical and SAR images for CC. The dataset for ground range detected (GRD) with Sentinel-1 SAR was acquired through the GEE cloud platform, containing all images of

the study area between January to April 2022. The study employed interference wideband mode with incidence angle variation of 35° to 40° to acquire the Sentinel-1 SAR GRD dataset, having a spatial resolution of 10 m and breadth of 250 km. The images underwent preprocessing on the GEE platform within the Sentinel-1 toolbox. To maintain image sharpness and minimize speckle, a refined Lee filter [32] was utilized to filter the Sentinel-1 images on the GEE platform.

3.1.2. Sentinel-2 data acquisition and preprocessing

To conduct research, we utilized Sentinel-2 orthorectified images from the GEE platform. The images were acquired between January to April 2022 over villages of Bhujla and Warud in Pusad, Maharashtra. Images were collected as a part of the Sentinel-2 multi-spectral instrument (MSI) level-1C dataset. The dataset consists of 13 top-of-atmosphere reflectance MSI bands, which are scaled by a factor of 1,000. We also used the quality assessment band (QA60) to exclude any invalid observations.

3.1.3. Field data

Between January and April 2022, a team of researchers visited the villages of Bhujla and Warud in Pusad, Maharashtra to collect field data about crop type and land cover. They used a GPS device to record the centre and four corners coordinates of each farm, in addition to the name of the crop and supplementary data about vegetation and structures within each farm. Wheat, chickpea, and watermelon were among the crops observed and recorded. After the field survey, the GPS coordinates of farm boundaries were uploaded into ArcGIS as a point shapefile and overlaid onto the GEE for downloading the Sentinel-1 and Sentinel-2 datasets. 70% of the collected ground truth data was applied to train the machine learning model, while the remaining 30% was used for validation.

3.2. Data preparation

3.2.1. Optical features

The growth of crops can be assessed through spectral indices that are sensitive to vegetation. The NDVI is highly responsive to leaf area index and chlorophyll present in crops which makes it an ideal metric to evaluate the greenness of vegetation [33], [34]. A research study has found that the MNDWI can effectively differentiate between open surface water bodies and vegetation and soils [35]. GNDVI is highly sensitive to chlorophyll, according to research [36], [37]. In recent years, the NDVI has been extensively utilized for calculating foliage cover [38]. Apart from the original Sentinel-2 bands, four prominent vegetation indices were calculated, including the NDVI, NDVI, GNDVI, and MNDWI.

$$NDVI = \frac{NIR - RED}{NIR + RED} \quad (1)$$

$$GNDVI = \frac{NIR - GREEN}{NIR + GREEN} \quad (2)$$

$$NDVI = \frac{GREEN - BLUE}{GREEN + BLUE} \quad (3)$$

$$MNDWI = \frac{GREEN - SWIR}{GREEN + SWIR} \quad (4)$$

3.2.2. Radar feature

Once the SAR image was acquired using GEE platform, VV and VH bands were extracted for CC. Rain and cloud cover don't affect SAR, which is capable of taking images day and night. The study fully utilized the benefits of SAR pictures by utilizing all winter wheat observation. Plant growth cycle-related changes in the water content of the canopy are reflected in VV and VH. band hence VV and VH provide more information about crop structure and characteristics, significantly improving CC algorithms' accuracy.

3.3. Crop classification

3.3.1. Different feature combinations

Several optical and radar feature combinations were evaluated for the purpose of comparison. The gamma and cost parameters are suitably tuned by the RF algorithm using a grid search and 8-fold cross-validation based on the training data. Next, we performed the RF for every combination of data. The performance of each model was compared by examining the overall accuracy (OA), producer's accuracy (PA), user's accuracy (UA), and Kappa coefficient (KC), following different combinations of optical and microwave features were explored to identify the most important radar and optical features for accurate crop mapping.

Combination 1: VH, VV SAR features
 Combination 2: Sentinel-2 bands
 Combination 3: Sentinel-2 bands and NDVI
 Combination 4: Sentinel-2 bands and GNDVI
 Combination 5: Sentinel-2 and NDYI
 Combination 6: Sentinel-2 and MNDWI
 Combination 7: Only Sentinel-2 bands and NDVI, GNDVI, NDYI and MNDWI
 Combination 8: With the fusion of all Sentinel-1 and Sentinel-2 features.

3.3.2. Pixel based classification

Conventional PB classification is a popular method for generating crop maps. The PB classification is performed at the pixel level, which solely relies on the spectral data of individual pixels. In PB classification, each pixel, the smallest unit in the image, is categorized into a predefined class using a trained model. Salt and pepper noise could be produced by the conventional PB categorization approach, particularly for Sentinel-1 radar data. This issue is lessened by the object-based approach, which divides the image into distinct regions or objects based on predetermined criteria by taking into account the neighboring information of a given pixel.

3.3.3. Object based classification

State-of-the-art machine learning algorithms can execute PB and OO classification methods on GEE. In the study presented, an RF classifier was used to implement PB and OO classification approaches, with the number of trees set to 100. An inbuilt GEE image segmentation algorithm was used to implement SNIC image segmentation, which is an OO imagery segmentation method that groups spatial objects with high uniformity. First, a centroid pixel initialization is done on the image's regular grid. Then, the dependence of each pixel with respect to the centroid is ascertained using the distance between pixels in the five-dimensional space of colour and spatial coordinates. Ultimately, the distance creates effective, compact, and almost uniform polygons by integrating the normalised spatial and colour distances [19], [31].

The SNIC algorithm was used to compare the performance of optical and SAR features for PB classification. The algorithm generates a regular grid of seeds using the "Image.Segmentation.seedGrid" function. The spacing of superpixel seed locations affects the cluster size and can be adjusted to achieve the best results. The algorithm was tested for different values of seed spacing to determine the best value based on OA. To produce compact clusters, the "compactness factor" parameter was set to a higher value, while the "connectivity" parameter was set to 8 to avoid tile boundary artifacts. Additionally, a "neighbourhoods" parameter was used to ensure that the tiles did not overlap. In this study, the SNIC parameters were set to compactness = 0, connectivity = 8, and neighbourhood size = 256. Finally, the visualization scale was found to significantly impact the accuracy of the SNIC algorithm for OO classification.

3.3.4. Random forest classifier

RF is a supervised machine learning model that does not follow the normal distribution of predictor variables. It integrates large decision trees and employs an adjustable amount of predictor variables. RF is built using the bootstrapping technique, where each decision tree is fitted based on in-bag data. For classification, two variables are to be set for the RF classifier, ntree which stands for the number of decision trees grown and mtry, which stands for the number of variables used at every split. A tree is trimmed only after it is fully developed and when its nodes are pure and can be used for prediction. RF was selected for its advantages, including the ability to handle large data sets, resistance to noise and outliers, and low computational complexity compared to other ensemble methods [39].

3.4. Accuracy assesement

The following metrics are employed to assess the algorithm presented in this work: OA, KC, UA, and PA. The OA is determined by calculating the ratio of correctly classified cells to the total number of cells [40]. The KC is a statistical measure of interclass agreement that assesses classification accuracy using all data available in the confusion matrix. The PA of a map is defined from the map producer's point of view, whereas UA is defined from the user's point of view [36], [40]. The formulas for OA, KC, PA and UA are given by expression (5)-(8) respectively.

$$OA = \frac{\sum_{i=1}^N m_{ii}}{\sum_{j=1}^N \sum_{i=1}^N m_{ij}} \quad (5)$$

$$KC = \frac{N \sum_{i=1}^n m_{ij} - \sum_{i=1}^n (m_i + m + i)}{N^2 - \sum_{i=1}^n (m_i + m + i)} \quad (6)$$

The PA of a map is defined from the map producer's point of view, whereas UA is defined from the user's point of view [36], [40]. The formulas for PA and UA are given in (7) and (8).

$$PA = \frac{m_{ii}}{m_{+i}} \quad (7)$$

$$UA = \frac{m_{ii}}{m_{i+}} \quad (8)$$

4. RESULTS AND DISCUSSION

4.1. Analysis of temporal signatures of optical data

In Figures 2(a) to 2(d), the temporal variation of NDVI, NDYI, GNDVI, and MNDWI of different classes (chickpea, wheat, watermelon, garlic, urban, and water) were plotted to study the temporal pattern of vegetation indexes at different phenological stages of various crops.

- The NDVI is a measure of vegetation cover that ranges from -1 to +1. In this scale, positive values indicate areas covered by clouds and water, while a value of 0 represents no vegetation cover. NDVI values that are close to 1 indicate dense vegetation. This index has been proven to be a helpful tool in estimating crop yield and monitoring crop growth. During the sowing period, crops typically have a small NDVI value. However, as they enter the fast-growing season, the NDVI value increases rapidly. Wheat, for instance, begins to mature from the end of February, and as it does so, its NDVI value decreases, reaching a minimum at harvesting time. Chickpea and wheat typically have NDVI values of more than 0.3, while the NDVI of other crops, urban areas, and water bodies are lower than 0.3. The water class usually shows the lowest NDVI values.
- Based on the blue and green bands, the NDYI is suitable for representing the increase in yellowness during blossoming. This is because flowers absorb a significant amount of blue light, and the high reflectance in the green and red bands is then perceived as yellow. The study found that in-situ data regarding the beginning and end of flowering was similar to that captured by the Sentinel-1 data [38].
- GNDVI has a temporal pattern similar to NDVI. However, it is a variation of NDVI that uses green reflectance instead of red.
- MNDWI can distinguish water and urban areas easily because water has the highest MNDWI value compared to other classes, while urban areas have negative MNDWI.

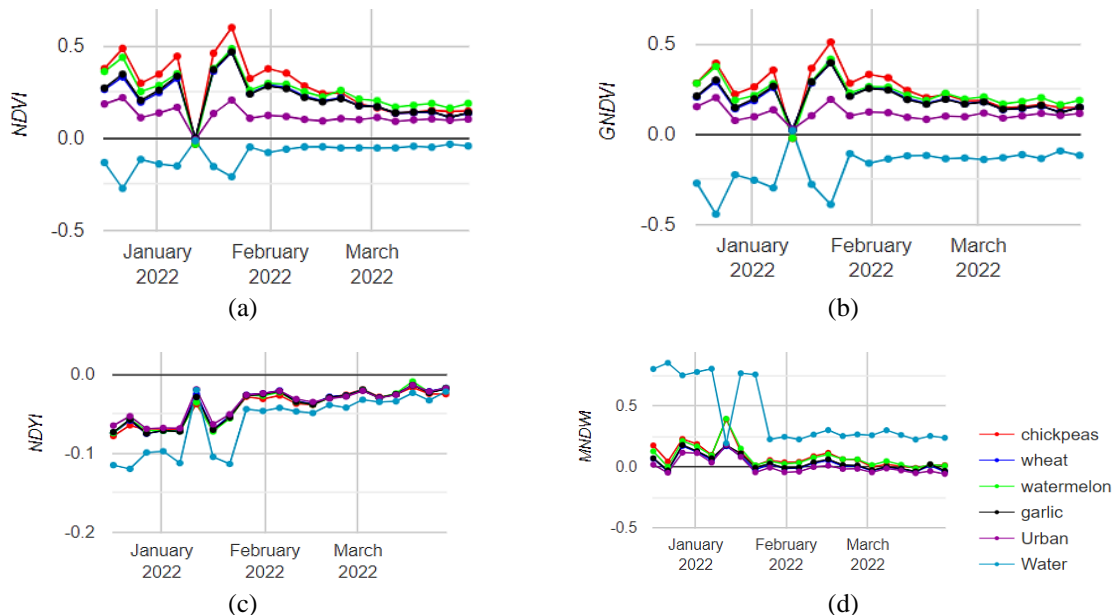


Figure 2. Temporal profiles of (a) NDVI, (b) GNDVI, (c) NDYI, and (d) MNDWI

4.2. Dynamics of SAR polarisations vertical-vertical and vertical-horizontal

The SAR VV and VH backscatter varies as the crop grows from sowing to harvesting. Figures 3(a) and 3(b) shows the temporal variation of the average backscatter coefficients of wheat, chickpea,

watermelon, garlic, water, and urban area under study in 2022. In Figure 3, on the X axis, the date of SAR image acquisition is taken, and on the Y axis value of the backscattering coefficient is placed.

- During the initial growth stages, backscatter values are low, however, they increase rapidly as crops progress to the vegetative stage.
- During the reproductive stage, slight variations in crop biomass and structure cause minute variation in backscatter.
- During harvesting, a significant decrease in backscatter was observed as the plant died, resulting in a reduction of the plant's water content. The backscatter dropped from -15 dB (VH), -7.5dB (VV) to -22 dB (VH), -11 dB (VV) for chickpea; -13dB (VH), -10 dB (VV) to -15 dB (VH), -13 dB (VV) for wheat; and -15 dB (VH), -10dB (VV) to -18 dB (VH), -12 dB (VV) for watermelon.
- The water class had the lowest backscatter and VV polarization showed higher backscatter variation as crops grew compared to VH polarization, this agrees with previous research [41].

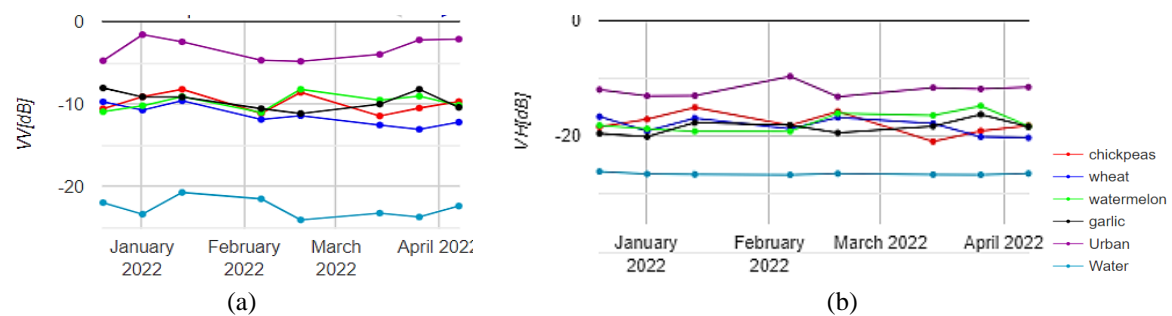


Figure 3. Temporal profiles of (a) vertical vertical (b) vertical horizontal

4.3. Classification results

The classification maps generated applying the proposed method for the investigation area are displayed in Figure 4. Figure 4(a) shows classification maps generated using PB method and Figure 4(b) shows classification maps generated using OO method. Table 1 lists the OAs and KC of the different classification schemes using Sentinel-1 and Sentinel-2 data. The OA results varied from 61% to 85.5% depending on the approach (PB or OO) and input features. The highest OA and KC of 85.5% and 0.774 was obtained for OO-based classification approach with the fusion of Sentinel-1 and Sentinel-2 data. On the other hand, only Sentinel-2 bands produced the lowest OA of 61% and KC of 0.37. Orynbaikyzy *et al.* [15] observed that Sentinel-1 data showed more promising results than Sentinel-2. This result was consistent with the conclusion of the proposed work. Verma *et al.* [12] used joint Sentinel-1 and Sentinel-2 data for CC, which yielded an OA of 83.87 and a KC of 0.78. Research by Yang *et al.* [19], the highest accuracy of 83.35% was obtained for CC based on the joint use of Sentinel-1 and Sentinel-2 images. Chickpea had the lowest UA and PA due to the smaller number of visited plots. Therefore, Chickpea was misclassified as other crops. This misclassification may have resulted from the coinciding growth stages of these crops.

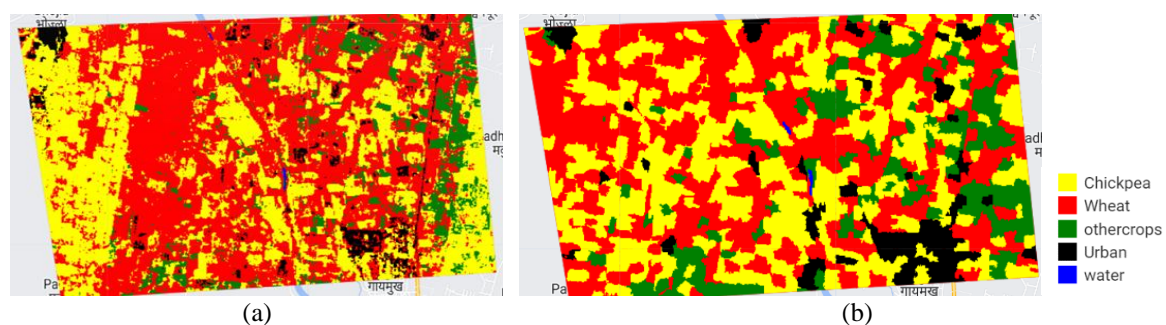


Figure 4. Using fusion of optical and SAR images (a) PB classification (b) OO classification approach

Table 1. OA and KP of each combination

Combination	PB		OO	
	OA	KC	OA	KC
VV+VH	0.8	0.69	0.83	0.76
Sentinel-2 bands	0.61	0.37	0.66	0.48
Sentinel-2 + NDVI	0.67	0.47	0.663	0.48
Sentinel-2 + GNDVI	0.679	0.47	0.664	0.481
Sentinel-2 + MNDVI	0.66	0.49	0.661	0.4879
Sentinel-2 + NDYI	0.6818	0.478	0.66	0.48
Sentinel-1 + Sentinel-2	0.8136	0.70	0.855	0.774

In the study, Figures 5(a) and 5(b) displays the UA and PA obtained for different categories using PB and OO classification techniques. The results indicate that the OO classification approach had a higher UA than the PB classification. The researchers concluded that the fusion of Sentinel-1 radar and Sentinel-2 optical data has resulted in an enhancement in accuracy of CC. Similar outcomes were also achieved in the studies [13], [14]. The OA obtained in this study was higher than [12], primarily due to the integration of Sentinel-1 and Sentinel-2 using the OO classification approach. Object-based CC eliminates object spectral variability by averaging many pixel values leading to an increase in accuracy. An important factor affecting the classification accuracy of high-resolution images classified using SNIC technique is the size of the superpixels. To increase the accuracy and efficiency of classification, the automatic optimal superpixel segmentation size selection method still has to be created.

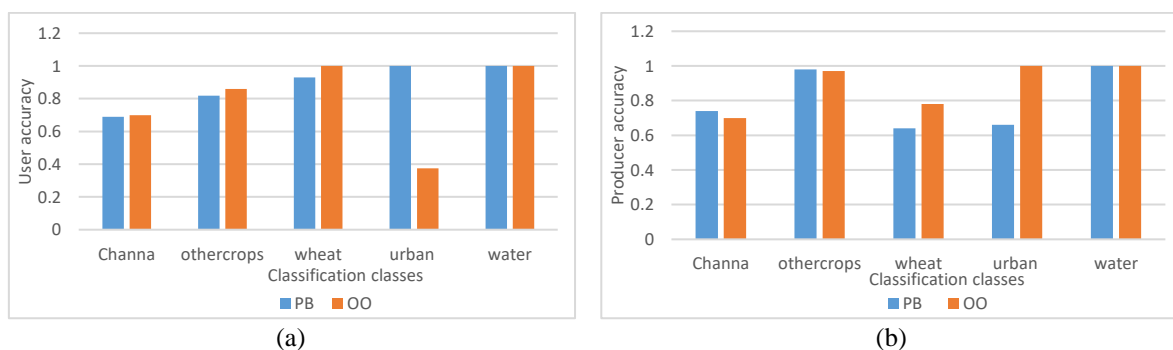


Figure 5. PB and OO classification of (a) user accuracy and (b) producer accuracy

5. CONCLUSION

The reason behind the investigation was to examine the potential of combining multi-temporal Sentinel-1 and optical Sentinel-2 images to map crops using the PB and OO classification approach with a RF classifier. Different combinations of optical and microwave features were explored to identify the most important radar and optical features for accurate crop mapping. The outcome demonstrated that the integration of Sentinel-1 and Sentinel-2 using the OO classification approach provided the best results. The RF model trained using the fusion of Sentinel-1 and Sentinel-2 data had a maximum OA of 85.53% and a KC of 0.77, which was higher than the OA obtained using either Sentinel-1 or Sentinel-2 data alone. This suggests that merging remote sensing data has excellent prospects for image segmentation and classification algorithms. The proposed method used GEE, which made the generation of crop maps convenient, fast and accurate. This approach is suitable for finely classifying crops in quite complex and heterogeneous regions. In the future, automatic selection of an ideal superpixel for SNIC can be explored to further boost the accuracy of the CC.

REFERENCES





- [1] J. Schmedtmann and M. Campagnolo, "Reliable crop identification with satellite imagery in the context of common agriculture policy subsidy control," *Remote Sensing*, vol. 7, no. 7, pp. 9325–9346, 2015, doi: 10.3390/rs70709325.
- [2] K. Van Tricht, A. Gobin, S. Gilliams, and I. Piccard, "Synergistic use of radar sentinel-1 and optical sentinel-2 imagery for crop mapping: A case study for Belgium," *Remote Sensing*, vol. 10, no. 10, 2018, doi: 10.3390/rs10101642.
- [3] M. A. Altieri, F. R. Funes-Monzote, and P. Petersen, "Agroecologically efficient agricultural systems for smallholder farmers: contributions to food sovereignty," *Agronomy for Sustainable Development*, vol. 32, no. 1, pp. 1–13, 2012, doi: 10.1007/s13593-011-0065-6.

- [4] C. Luo, H. Liu, L. Lu, Z. Liu, F. Kong, and X. Zhang, "Monthly composites from sentinel-1 and sentinel-2 images for regional major crop mapping with Google Earth Engine," *Journal of Integrative Agriculture*, vol. 20, no. 7, pp. 1944–1957, 2021, doi: 10.1016/S2095-3119(20)63329-9.
- [5] M. Berger, J. Moreno, J. A. Johannessen, P. F. Levelt, and R. F. Hanssen, "ESA's sentinel missions in support of Earth system science," *Remote Sensing of Environment*, vol. 120, pp. 84–90, 2012, doi: 10.1016/j.rse.2011.07.023.
- [6] N. Gorelick, M. Hancher, M. Dixon, S. Ilyushchenko, D. Thau, and R. Moore, "Google Earth Engine: Planetary-scale geospatial analysis for everyone," *Remote Sensing of Environment*, vol. 202, pp. 18–27, 2017, doi: 10.1016/j.rse.2017.06.031.
- [7] G. T. Desai and A. N. Gaikwad, "Automatic land cover classification with SAR imagery and machine learning using Google Earth Engine," *International journal of electrical and computer engineering systems*, vol. 13, no. 10, pp. 909–916, 2022, doi: 10.32985/ijeces.13.10.6.
- [8] A. E. Maxwell, T. A. Warner, and F. Fang, "Implementation of machine-learning classification in remote sensing: an applied review," *International Journal of Remote Sensing*, vol. 39, no. 9, pp. 2784–2817, 2018, doi: 10.1080/01431161.2018.1433343.
- [9] D. J. Lary, A. H. Alavi, A. H. Gandomi, and A. L. Walker, "Machine learning in geosciences and remote sensing," *Geoscience Frontiers*, vol. 7, no. 1, pp. 3–10, 2016, doi: 10.1016/j.gsf.2015.07.003.
- [10] M. Belgiu and L. Drăguț, "Random forest in remote sensing: A review of applications and future directions," *ISPRS Journal of Photogrammetry and Remote Sensing*, vol. 114, pp. 24–31, 2016, doi: 10.1016/j.isprsjprs.2016.01.011.
- [11] A. Veloso et al., "Understanding the temporal behavior of crops using sentinel-1 and sentinel-2-like data for agricultural applications," *Remote Sensing of Environment*, vol. 199, pp. 415–426, 2017, doi: 10.1016/j.rse.2017.07.015.
- [12] A. Verma, A. Kumar, and K. Lal, "Kharif crop characterization using combination of SAR and MSI optical sentinel satellite datasets," *Journal of Earth System Science*, vol. 128, no. 8, 2019, doi: 10.1007/s12040-019-1260-0.
- [13] A. Chakhar, D. Hernández-López, R. Ballesteros, and M. A. Moreno, "Improving the accuracy of multiple algorithms for crop classification by Integrating sentinel-1 observations with sentinel-2 data," *Remote Sensing*, vol. 13, no. 2, 2021, doi: 10.3390/rs13020243.
- [14] Y. Chen, J. Hou, C. Huang, Y. Zhang, and X. Li, "Mapping maize area in heterogeneous agricultural landscape with multi-temporal sentinel-1 and sentinel-2 images based on random forest," *Remote Sensing*, vol. 13, no. 15, 2021, doi: 10.3390/rs13152988.
- [15] A. Orynbaiyzy, U. Gessner, B. Mack, and C. Conrad, "Crop type classification using fusion of sentinel-1 and sentinel-2 data: Assessing the impact of feature selection, optical data availability, and parcel sizes on the accuracies," *Remote Sensing*, vol. 12, no. 17, 2020, doi: 10.3390/rs12172779.
- [16] R. Sonobe, Y. Yamaya, H. Tani, X. Wang, N. Kobayashi, and K. Mochizuki, "Assessing the suitability of data from sentinel-1A and 2A for crop classification," *GIScience & Remote Sensing*, vol. 54, no. 6, pp. 918–938, 2017, doi: 10.1080/15481603.2017.1351149.
- [17] V. Walter, "Object-based classification of remote sensing data for change detection," *ISPRS Journal of Photogrammetry and Remote Sensing*, vol. 58, no. 3–4, pp. 225–238, 2004, doi: 10.1016/j.isprsjprs.2003.09.007.
- [18] M. Baatz, C. Hoffmann, and G. Willhauck, "Progressing from object-based to object-oriented image analysis," in *Object-Based Image Analysis*, Springer Berlin Heidelberg, 2008, pp. 29–42.
- [19] L. Yang, L. Wang, G. A. Abubakar, and J. Huang, "High-resolution rice mapping based on SNIC segmentation and multi-source remote sensing images," *Remote Sensing*, vol. 13, no. 6, 2021, doi: 10.3390/rs13061148.
- [20] N.-T. Son, C.-F. Chen, C.-R. Chen, and V.-Q. Minh, "Assessment of sentinel-1A data for rice crop classification using random forests and support vector machines," *Geocarto International*, pp. 1–15, 2017, doi: 10.1080/10106049.2017.1289555.
- [21] M. A. Nihar, J. M. Ahamed, S. Pazhanivelan, R. Kumaraperumal, and K. G. Raj, "Estimation of cotton and maize crop area in Perambalur District Of Tamil Nadu using multi-date sentinel-1A SAR data," *The International Archives of the Photogrammetry, Remote Sensing and Spatial Information Sciences*, pp. 67–71, 2019, doi: 10.5194/isprs-archives-XLII-3-W6-67-2019.
- [22] P. P. D. Bem, O. A. D. C. Júnior, O. L. F. D. Carvalho, R. A. T. Gomes, R. F. Guimarães, and C. M. M. Pimentel, "Irrigated rice crop identification in Southern Brazil using convolutional neural networks and sentinel-1 time series," *Remote Sensing Applications: Society and Environment*, vol. 24, 2021, doi: 10.1016/j.rsase.2021.100627.
- [23] L. E. C. L. Rosa, R. Q. Feitosa, P. N. Happ, I. D. Sanches, and G. A. O. P. D. Costa, "Combining deep learning and prior knowledge for crop mapping in tropical regions from multitemporal SAR image sequences," *Remote Sensing*, vol. 11, no. 17, 2019, doi: 10.3390/rs11172029.
- [24] E. Ndikumana, D. H. T. Minh, N. Baghdadi, D. Courault, and L. Hossard, "Deep recurrent neural network for agricultural classification using multitemporal SAR sentinel-1 for Camargue, France," *Remote Sensing*, vol. 10, no. 8, 2018, doi: 10.3390/rs10081217.
- [25] N. Kobayashi, H. Tani, X. Wang, and R. Sonobe, "Crop classification using spectral indices derived from sentinel-2A imagery," *Journal of Information and Telecommunication*, vol. 4, no. 1, pp. 67–90, 2020, doi: 10.1080/24751839.2019.1694765.
- [26] R. Saini and S. K. Ghosh, "Crop classification on single date sentinel-2 imagery using random forest and support vector machine," *The International Archives of the Photogrammetry, Remote Sensing and Spatial Information Sciences*, vol. XLII–5, pp. 683–688, 2018, doi: 10.5194/isprs-archives-XLII-5-683-2018.
- [27] R. Sonobe, Y. Yamaya, H. Tani, X. Wang, N. Kobayashi, and K. Mochizuki, "Crop classification from sentinel-2-derived vegetation indices using ensemble learning," *Journal of Applied Remote Sensing*, vol. 12, no. 02, 2018, doi: 10.1117/1.JRS.12.026019.
- [28] V. Mazzia, A. Khaliq, and M. Chiaberge, "Improvement in land cover and crop classification based on temporal features learning from sentinel-2 data using recurrent-convolutional neural network (R-CNN)," *Applied Sciences*, vol. 10, no. 1, 2019, doi: 10.3390/app10010238.
- [29] M. Fauvel, Y. Tarabalka, J. A. Benediktsson, J. Chanussot, and J. C. Tilton, "Advances in spectral-spatial classification of hyperspectral images," *Proceedings of the IEEE*, vol. 101, no. 3, pp. 652–675, 2013, doi: 10.1109/JPROC.2012.2197589.
- [30] Q. Yu, P. Gong, N. Clinton, G. Biging, M. Kelly, and D. Schirokauer, "Object-based detailed vegetation classification with airborne high spatial resolution remote sensing imagery," *Photogrammetric Engineering & Remote Sensing*, vol. 72, no. 7, pp. 799–811, 2006, doi: 10.14358/PERS.72.7.799.
- [31] C. Luo et al., "Using time series sentinel-1 images for object-oriented crop classification in Google Earth Engine," *Remote Sensing*, vol. 13, no. 4, 2021, doi: 10.3390/rs13040561.
- [32] J.-S. Lee, J.-H. Wen, T. L. Ainsworth, K.-S. Chen, and A. J. Chen, "Improved sigma filter for speckle filtering of SAR imagery," *IEEE Transactions on Geoscience and Remote Sensing*, vol. 47, no. 1, pp. 202–213, 2009, doi: 10.1109/TGRS.2008.2002881.
- [33] C. A. D. Vittorio and A. P. Georgakakos, "Land cover classification and wetland inundation mapping using MODIS," *Remote Sensing of Environment*, vol. 204, pp. 1–17, 2018, doi: 10.1016/j.rse.2017.11.001.





- [34] C. J. Tucker, "Red and photographic infrared linear combinations for monitoring vegetation," *Remote Sensing of Environment*, vol. 8, no. 2, pp. 127–150, 1979, doi: 10.1016/0034-4257(79)90013-0.
- [35] H. Xu, "Modification of normalised difference water index (NDWI) to enhance open water features in remotely sensed imagery," *International Journal of Remote Sensing*, vol. 27, no. 14, pp. 3025–3033, 2006, doi: 10.1080/01431160600589179.
- [36] M. F. Isip, R. T. Alberto, and A. R. Biagtan, "Exploring vegetation indices adequate in detecting twister disease of onion using sentinel-2 imagery," *Spatial Information Research*, vol. 28, no. 3, pp. 369–375, 2020, doi: 10.1007/s41324-019-00297-7.
- [37] W. Wu, "The generalized difference vegetation index (GDVI) for dryland characterization," *Remote Sensing*, vol. 6, no. 2, pp. 1211–1233, 2014, doi: 10.3390/rs6021211.
- [38] G. Misra, F. Cawkwell, and A. Wingler, "Status of phenological research using sentinel-2 data: a review," *Remote Sensing*, vol. 12, no. 17, p. 2760, 2020, doi: 10.3390/rs12172760.
- [39] V. F. Rodriguez-Galiano, B. Ghimire, J. Rogan, M. Chica-Olmo, and J. P. Rigol-Sanchez, "An assessment of the effectiveness of a random forest classifier for land-cover classification," *ISPRS Journal of Photogrammetry and Remote Sensing*, vol. 67, pp. 93–104, 2012, doi: 10.1016/j.isprsjprs.2011.11.002.
- [40] Z. Wang, L. Xu, Q. Ji, W. Song, and L. Wang, "A multi-level non-uniform spatial sampling method for accuracy assessment of remote sensing image classification results," *Applied Sciences*, vol. 10, no. 16, 2020, doi: 10.3390/app10165568.
- [41] A. Tassi, D. Gigante, G. Modica, L. Di Martino, and M. Vizzari, "Pixel- vs. object-based landsat 8 data classification in Google Earth Engine using random forest: the case study of Maiella National Park," *Remote Sensing*, vol. 13, no. 12, 2021, doi: 10.3390/rs13122299.

BIOGRAPHIES OF AUTHORS



Geeta T. Desai     received her B.E. degree from Padre Conceicao College of Engineering, Verna, Goa University, M.E. in electronics and telecommunication engineering from the Mumbai University in 2014, and completed her Ph.D. degree in electronics from Babasaheb Naik College of Engineering, Pusad from Amravati university. She is working as an Assistant Professor in Department of Electronics and Computer, in Anjuman-I-Islam's Kalsekar Technical Campus. Her current research interests include digital image processing, remote sensing, and machine learning. She can be contacted at email: tgeetadesai@gmail.com.



Abhay N. Gaikwad     received his B.E. degree from Babasaheb Naik College of Engineering, Pusad, Amravati University, Amravati in 1993, M.Tech. from VNIT (formerly VRCE) Nagpur in 2001 and Ph.D. from Indian Institute of Technology, Roorkee, Uttarakhand, India in 2012. He is presently working as Head of Department of Artificial Intelligence and Data Science Engineering, Babasaheb Naik College of Engineering Pusad. He has 29 years of experience in teaching. His research interest includes wireless communication, radar signal processing, through wall imaging radar, and machine learning. He can be contacted at email: abhay.n.gaikwad@gmail.com.